

# Dynamical Correlation Functions using the Density Matrix Renormalization Group

Till D. Kühner<sup>1,2</sup> and Steven R. White<sup>1</sup>

<sup>1</sup>*Department of Physics and Astronomy, University of California, Irvine, CA 92697*

<sup>2</sup>*Physikalisches Institut der Universität Bonn, D-53115 Bonn, Germany*

(April 26, 2024)

The density matrix renormalization group (DMRG) method allows for very precise calculations of ground state properties in low-dimensional strongly correlated systems. We investigate two methods to expand the DMRG to calculations of dynamical properties. In the Lanczos vector method the DMRG basis is optimized to represent Lanczos vectors, which are then used to calculate the spectra. This method is fast and relatively easy to implement, but the accuracy at higher frequencies is limited. Alternatively, one can optimize the basis to represent a correction vector for a particular frequency. The correction vectors can be used to calculate the dynamical correlation functions at these frequencies with high accuracy. By separately calculating correction vectors at different frequencies, the dynamical correlation functions can be interpolated and pieced together from these results. For systems with open boundaries we discuss how to construct operators for specific wavevectors using filter functions.

## I. INTRODUCTION

Since its development, the density matrix renormalization group<sup>1,2</sup> (DMRG) has been successfully used to calculate static properties of ground states and low-lying excited states in various low dimensional strongly interacting systems. Energies can be determined with highest precision, and the calculation of time-independent correlation functions is easy and high accuracy can be achieved. The calculation of dynamical properties is more difficult.

The Lanczos vector method, also known as the continued fractions method, can be used to determine the dynamical correlation functions in an exact diagonalization calculation. However, in a DMRG calculation, if the basis is optimized only to represent the ground state, this will lead to poor results, since the Lanczos vectors are not represented correctly in the truncated basis. Hallberg suggested using several of the first Lanczos vectors as target states in addition to the ground state<sup>3</sup>. Reasonable results were obtained for an  $S=1/2$  chain, but the true accuracy of the method was not determined, since the infinite system DMRG method, rather than the finite system method, was used. In this paper we determine the accuracy of this method for the more appropriate finite system method.

An alternative approach for generating dynamical spectra is the correction vector method, which yields exact results within the given basis<sup>4</sup>. Although it has been used in the DMRG context<sup>5</sup>, in those calculations the basis was not expanded to represent these correction vectors. Here we apply the correction vector method, targeting a correction vector at a particular frequency. We find that the dynamical correlation function at this frequency can be calculated directly and very accurately. We show how to piece together results from correction vectors at different frequencies to obtain the full spectrum.

Taking antiferromagnetic Heisenberg chains with spin 1 and spin  $1/2$  as examples, we discuss the advantages

and limitations of the two methods. We show how to obtain the spectral weight functions, and how to judge the quality of the numerical results.

DMRG calculations are most accurate with open boundary conditions, in which case momentum is not precisely defined. In this work we show how to construct operators corresponding to wavevectors in systems with open boundaries using filter functions.

In Section II we discuss the construction of the operators for systems with open boundaries. In Section III we present the Lanczos method, and in Section IV we apply it to the antiferromagnetic spin-1 chain. As an example where the Lanczos method does not work so well we discuss the antiferromagnetic spin-1/2 chain in Section V. In Section VI we present the correction vector method, and we give conclusions in Section VII.

## II. CONSTRUCTION OF OPERATORS FOR OPEN SYSTEMS

To calculate a Green's function

$$G(q, z) = \langle 0 | A_q^\dagger \frac{1}{z - H} A_q | 0 \rangle \quad (1)$$

with  $z = \omega + i\eta$ , we have to be able to apply an operator  $A_q$  in our system. The DMRG works in real-space, and operators with wavevectors  $q$  can be obtained as Fourier transforms of on-site operators  $A_n$ . In infinite systems they are given as:

$$A_q = \sum_{n=-\infty}^{\infty} A_n e^{ix_n q}, \quad (2)$$

$$A_n = \frac{1}{2\pi} \int_{-\pi}^{\pi} dq A_q e^{-ix_n q}. \quad (3)$$

where  $x_n$  is the position of site  $n$ , the lattice spacing is  $a = 1$ .

For finite systems with open boundaries, we construct operators defined as wavepackets, with finite spatial extent and finite uncertainty in the momentum. We construct the wavepacket by inserting a windowing or filter function in Eq.(2). If only real operators are used, it is numerically convenient to construct

$$A(q) = \sum_{n=-\infty}^{\infty} \sin(qx_n) f(x_n) A_n = \frac{1}{4\pi i} \int dq' (A_{q'} - A_{-q'}) f(q - q'), \quad (4)$$

and

$$A(q) = \sum_{n=-\infty}^{\infty} \cos(qx_n) f(x_n) A_n = \frac{1}{4\pi} \int dq' (A_{q'} + A_{-q'}) f(q - q') \quad (5)$$

where  $f(x_n) = F(\frac{x_n}{M})$  is the filter function,  $2M$  is the width of the window. We use system with even numbers of sites, and  $x_n$  is offset so that  $x = 0$  is in the center of the system. The sites closest to the middle of the system are at  $x = -1/2$  and  $x = 1/2$ . The operators  $A(q)$  are reflection symmetric, which allows, if the Hamiltonian is also reflection symmetric, using reflected system blocks as environment blocks in the DMRG.

Applying the operator as if the system were periodic, is equivalent to using a rectangular window  $F^r(x)$  as the filter function with  $2M = L$ :

$$F^r(x) = \begin{cases} 1 & \text{if } -1 \leq x \leq 1 \\ 0 & \text{otherwise} \end{cases} \quad (6)$$

This operator is seriously flawed. First, it has substantial weight at the edges of the system, where open boundary effects are significant. Second, even if we ignore the edge effects, this window is very broad in the wavevector space. The Fourier transform of  $F^r(x)$  is

$$F^r(q) = \sin\left(\frac{Lq}{2}\right) \left( \sin\left(\frac{q}{2}\right) - \frac{\sin(q) \cos\left(\frac{q}{2}\right)}{\cos(q) - 1} \right), \quad (7)$$

which for small  $q$  is

$$F^r(q) \approx \frac{2 \sin(L/2q)}{q}. \quad (8)$$

The wavevector uncertainty  $\Delta q$  of this operator is of order 1, even when  $L \rightarrow \infty$ , whereas  $q$  itself ranges from 0 to  $2\pi$ . Therefore this operator is not useful.

As is well known from elementary quantum mechanics, the wavepacket with the minimum product of uncertainties  $\Delta q \Delta x$  is a Gaussian function. However, it is more desirable to use an operator which is equal to 0 at the edges of the system. A widely used filter that looks similar to a Gaussian in the center, but with compact support, is the Parzen filter (Fig. 1):

$$F_p(x) = \begin{cases} 1 - 6|x|^2 + 6|x|^3 & \text{if } 0 \leq |x| \leq 1/2 \\ 2(1 - |x|)^3 & \text{if } 1/2 \leq |x| \leq 1. \end{cases} \quad (9)$$

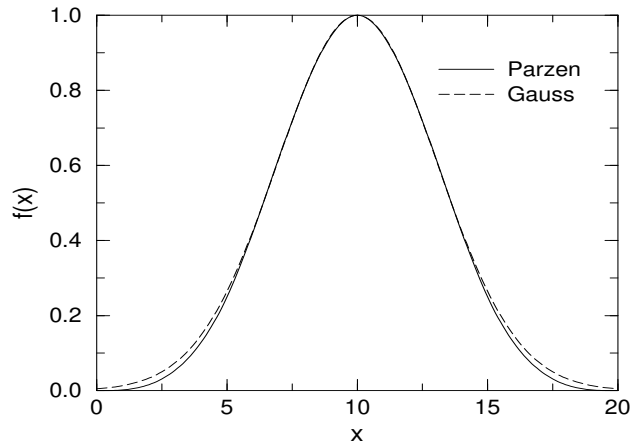


FIG. 1. Parzen and Gaussian functions in a  $L = 20$  site system. The halfwidth of the Parzen function is approximately  $0.18L$ . The Gaussian has a standard deviation of  $\sigma \approx 0.153L$ , while the standard deviation of the Parzen window, because of the faster decay of its tails, is only  $\sigma \approx 0.112L$ .

With  $2M = L$  this filter smoothly goes to zero at the boundaries. The Fourier transform is

$$F_p(q) \approx 24 \frac{3 + \cos(qM) - 4 \cos(qM/2)}{q^4 M^3} \quad (10)$$

and the wavevector uncertainty is  $\Delta q = 2\sqrt{3}/M$ . We see that  $\Delta q$  varies inversely with the system size if  $2M = L$ . For example, in a system with 100 sites  $\sigma \approx 0.07$ , and with wavevectors  $0 \leq q \leq 2\pi$  this is a relative error of only  $\Delta q = 1.1\%$ . Figure 2 shows how the Fourier transform of the Parzen filter smoothly goes to zero, while the Fourier transform of a rectangular window has oscillations at higher frequencies.

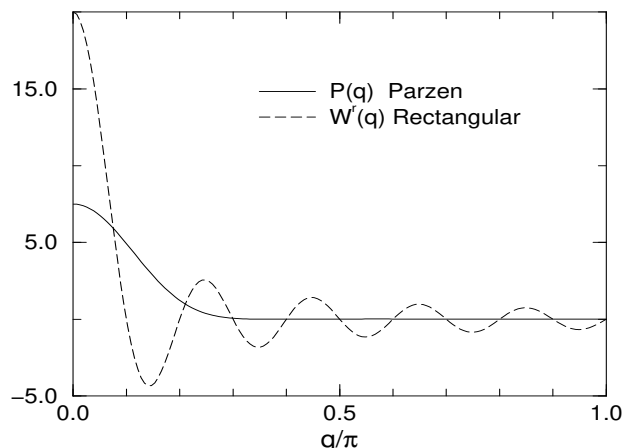


FIG. 2. The Fourier transform of the Parzen filter and the rectangular window. In real space both filters are 20 sites wide. It is obvious that the Parzen filter has a smaller width in wavevector space.

The use of sine (Eq. 4) and cosine (Eq. 5) functions for the operators instead of the complex form (Eq. 2) requires some special attention. The Green's function is

$$G(q, z) = \langle A^\dagger(q) \frac{1}{z-H} A(q) \rangle \\ = \frac{1}{4} \langle (A_q^\dagger \pm A_{-q}^\dagger) \frac{1}{z-H} (A_q \pm A_{-q}) \rangle. \quad (11)$$

with “−” for sine and “+” for cosine. Noting that  $\langle A_{-q}^\dagger \frac{1}{z-H} A_{-q} \rangle = \langle A_q^\dagger \frac{1}{z-H} A_q \rangle$  and  $A_{-\pi} = -A_\pi$ , there are three different cases for the Green's function. For  $A(q) = \sum_n \cos(qn) A_n$  it is:

$$G(q, z) = \begin{cases} \frac{1}{2} \langle A_q^\dagger \frac{1}{z-H} A_q \rangle & \text{for } 0 < q < \pi \\ \langle A_q^\dagger \frac{1}{z-H} A_q \rangle & \text{for } q = 0 \\ 0 & \text{for } q = \pi \end{cases} \quad (12)$$

For  $A(q) = \sum_n \sin(qn) A_n$ :

$$G(q, z) = \begin{cases} \frac{1}{2} \langle A_q^\dagger \frac{1}{z-H} A_q \rangle & \text{for } 0 < q < \pi \\ 0 & \text{for } q = 0 \\ \langle A_q^\dagger \frac{1}{z-H} A_q \rangle & \text{for } q = \pi \end{cases} \quad (13)$$

If only sine or cosine functions are used, the values found at  $q = 0$  and  $q = \pi$  are either zero or twice the expected values. By doing separate calculations with sine and cosine functions and adding up the results the correct values are always obtained.

In finite systems this effect is broadened due to the finite width  $\Delta q$  of the operators in the wavevector space. To get system size independent values for the Green's functions we require  $\pi^2 = \int dq f(q)^2$  for the filter functions. For the Parzen filter this means that an additional prefactor of  $\sqrt{\frac{140\pi}{151M}}$  must be included in the filter.

### III. LANCZOS VECTOR METHOD

To calculate spectral functions a Lanczos vector procedure can be used<sup>3</sup>. To do this, the Hamiltonian  $H$  is projected onto a Krylov subspace spanned by Lanczos vectors  $|f_n\rangle$ :

$$\begin{aligned} |f_0\rangle &= A_q|0\rangle / \langle 0|A_q^\dagger A_q|0\rangle \\ a_n &= \langle f_n|H|f_n\rangle \\ b_n &= \||r_n\rangle\|_2 \\ |r_n\rangle &= (H - a_n)|f_n\rangle - b_{n-1}|f_{n-1}\rangle \\ |f_{n+1}\rangle &= |r_n\rangle / b_n \end{aligned} \quad (14)$$

In the Lanczos basis the Hamiltonian is tridiagonal:

$$H = \begin{pmatrix} a_0 & b_0 & & & & 0 \\ b_0 & a_1 & b_1 & & & \\ & b_1 & a_2 & b_2 & & \\ & & \ddots & \ddots & \ddots & \\ & & & b_{n-2} & a_{n-1} & b_{n-1} \\ 0 & & & & b_{n-1} & a_n \end{pmatrix}$$

Now the eigenvectors  $|\Phi_n\rangle$  of  $H$  are used as an approximation of the identity  $1 \approx \sum_n |\Phi_n\rangle \langle \Phi_n|$ . Inserting this into the Green's function we get:

$$G(q, z) \approx \sum_{n,m} \langle 0|A_q^\dagger |\Phi_n\rangle \langle \Phi_n| \frac{1}{z-H} |\Phi_m\rangle \langle \Phi_m| A_q|0\rangle \\ = \sum_n \langle \Phi_n| \frac{1}{z-H} |\Phi_n\rangle \langle \Phi_n| A_q|0\rangle^2 \\ = \sum_n \frac{(\Phi_n^0)^2 \langle 0|A_q^\dagger A_q|0\rangle}{z - E_n} \quad (15)$$

Here  $E_n$  is the eigenvalue of  $\Phi_n$ , and  $\Phi_n^m = \langle f_n|\Phi_n\rangle$ . The dynamical correlation function  $I_A(q, \omega)$  is then given by

$$I_A(q, \omega) = -\frac{1}{\pi} \text{Im} \lim_{\eta \rightarrow 0^+} G(q, \omega + i\eta + E_g) \\ = \frac{\langle 0|A_q^\dagger A_q|0\rangle}{\pi} \lim_{\eta \rightarrow 0^+} \sum_n \frac{\eta (\Phi_n^0)^2}{(\omega + E_g - E_n)^2 + \eta^2} \\ = \langle 0|A_q^\dagger A_q|0\rangle \sum_n \delta(\omega + E_g - E_n) (\Phi_n^0)^2, \quad (16)$$

where  $E_g$  is the ground state energy. The peaks in the correlation function are at  $\omega_n = E_n - E_g$ .

The major source of errors in this is the approximation of the identity in terms of Lanczos vectors, and the small number  $N_L$  of these Lanczos vectors that can be used as target states in practical calculations. Only those states that are used as target states can be relied on as being represented correctly. Similar to the Lanczos algorithm for the solution of eigensystems, every additional Lanczos vector adds another peak, typically at high energy, while peaks with the smallest frequencies are determined most precisely and converge the fastest.

To obtain the dynamical correlation function at the end of the calculation, we make full use of the available Hilbert space. We calculate  $I(q, \omega)$  at the DMRG step where the system block is the same size as the environment block, since the truncation errors are smallest in that step. To do this, we not only use the Lanczos vectors that were target states, but keep calculating new Lanczos vectors until orthogonality breaks down and the overlap of the new Lanczos vector  $|f_n\rangle$  with the first Lanczos vector  $|f_0\rangle$  is bigger than 1%.

If more than just a few Lanczos vectors are used, the question of the weight that is assigned to these target states in the density matrix has to be addressed. The weight of a Lanczos vector in the spectrum is given by:

$$w_n = \sum_m (\Phi_m^0)^2 (\Phi_m^n)^2. \quad (17)$$

Taking this as a measure for the importance of a Lanczos vector, we assign 50% of the weight to the ground state, and distribute the remaining 50% among the Lanczos target states according to their weight  $w_n$ .

#### IV. THE SPIN 1 HEISENBERG MODEL

As an example we look at the antiferromagnetic spin 1 Heisenberg model:

$$H = \sum_i \vec{S}_i \vec{S}_{i+1}. \quad (18)$$

Each of the spins can be viewed as two spin-1/2 spins that pair with the spin-1/2 on the neighboring site in an antisymmetric singlet wavefunction<sup>6</sup>. In an open chain this effectively leaves unpaired spin-1/2's at the ends. To compensate for this, we add real spin-1/2's at the ends of the chain. We do not include these spins in the calculation of the spectra and set  $2M = L - 2$  for the Parzen filter.

This system has a finite correlation length  $\xi \approx 6.03(1)$  and the Haldane gap  $\Delta_H = 0.41050(2)^7$ , that separates the ground state from the first excitation, a single magnon with wavevector  $\pi$ . DMRG is particularly accurate in this system even if the number of states kept is small.

To obtain the dynamical correlation function we keep the ground state and the three first Lanczos states as target states ( $N_L = 3$ ), and we keep  $m = 128$  states in the DMRG basis. To verify that keeping three Lanczos vectors as target states is enough, we calculate the weight of the Lanczos vectors in the final  $S^+(q, \omega)$  for  $q = \pi$ . Figure 3 shows that the weight of the first vectors is big and decays fast, and the first three Lanczos vectors contain 98.87% of the total weight.

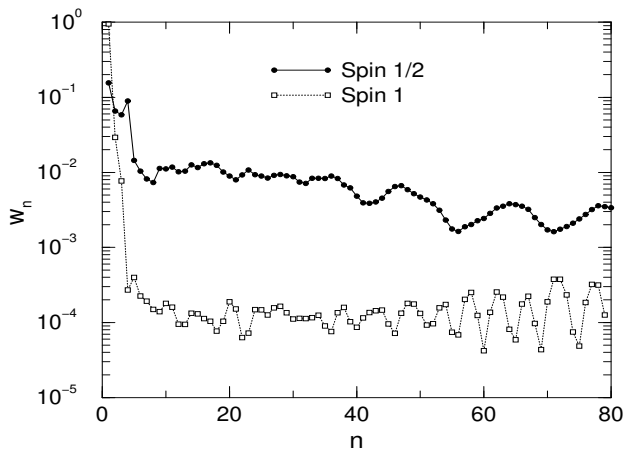


FIG. 3. The weight  $w_n$  of the Lanczos vectors in the spectrum.  $L = 320$ ,  $N_L = 3$  Lanczos target states,  $m = 128$  states for Spin 1 and  $m = 256$  states for Spin 1/2,  $q = \pi$ . Weight for the first three vectors:  $\sum_{n=0}^2 w_n = 0.2799$  for Spin 1/2, and  $\sum_{n=0}^2 w_n = 0.9887$  for Spin 1.

To further verify the convergence of the DMRG basis, we calculate  $S'^+(q, \omega)$  in every step and compare it to the final result  $S^+(q, \omega)$  by taking the inner product of the two:

$$\frac{S'^+(q) \cdot S^+(q)}{\|S'^+(q)\| \|S^+(q)\|}, \quad (19)$$

with the inner product defined as  $A \cdot B \equiv \int_{-\pi}^{\pi} d\omega A(\omega) B(\omega)$ , and the norm  $\|A\| = \sqrt{A \cdot A}$ . For this calculation we use a finite broadening factor  $\eta = 0.01$ . Figure 4 shows the product for every DMRG step. The discontinuities occur when the system and environment blocks have the same size, and utilizing reflection symmetry, the system block is reflected onto the environment block. After two sweeps the DMRG basis is converged, there are no further discontinuities, only small oscillations which are due to the different truncation effect depending on the size of the system and the environment block. Obviously with three Lanczos target states the spectrum is described well enough, and convergence is very good.

In the calculation of the final spectrum, Lanczos vectors are calculated until the overlap of the new vector with the first one exceeds 1%. The inset of Fig. 4 shows that the overlap  $\langle f_n | f_0 \rangle$  increases exponentially. In the given example we use the first 83 Lanczos vectors. It can be seen from the overlap that orthogonality breaks down after 95 Lanczos vectors have been calculated, effectively restarting the procedure. The effect on the resulting spectrum if more Lanczos vectors are used is very small.

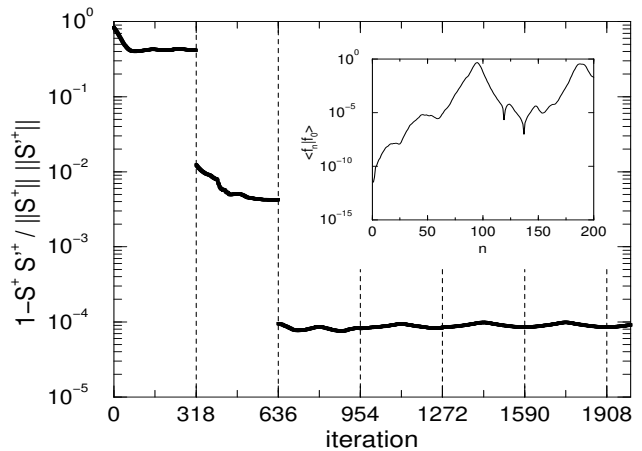


FIG. 4. Deviation from unity of the overlap of the spectral weight calculated in every step with the spectral weight calculated in the last step. Spectral weights at  $q = \pi$  in a 320 site long spin-1 chain, with a broadening factor  $\eta = 0.01$  and  $m = 128$  states kept. Iterations are counted from the first step after the build-up phase. The dashed lines indicate the iterations at which the system and environment block have the same size. The inset shows the overlap of the first Lanczos vector  $|f_0\rangle$  with  $|f_n\rangle$  in the final calculation of the correlation function.

Figure 5 shows  $S^+(q, \omega)$  for  $q = \pi$ . Most of the weight is in one single peak, and with increasing system size this peak moves towards the Haldane gap. To be sure that keeping  $m = 128$  states in the DMRG basis is enough, we compare results with those from calculations with  $m = 64$  and  $m = 256$  states. Table I shows the truncation error depending on the system size and number of states. The truncation errors are relatively small even with  $m = 64$  states, and the difference between those with  $m = 128$  and  $m = 256$  states are small.

TABLE I. The truncation error  $P(m)$  as a function of the length  $L$  of the spin-1 chain and the number  $m$  of states kept.

$L$	$P(m = 64)$	$P(m = 128)$	$P(m = 256)$
40	$1.1 \times 10^{-6}$	$2.1 \times 10^{-8}$	$1.2 \times 10^{-8}$
80	$1.6 \times 10^{-6}$	$3.0 \times 10^{-8}$	$3.5 \times 10^{-9}$
160	$1.7 \times 10^{-6}$	$3.2 \times 10^{-8}$	$8.6 \times 10^{-9}$
320	$1.5 \times 10^{-6}$	$3.2 \times 10^{-8}$	$3.0 \times 10^{-9}$

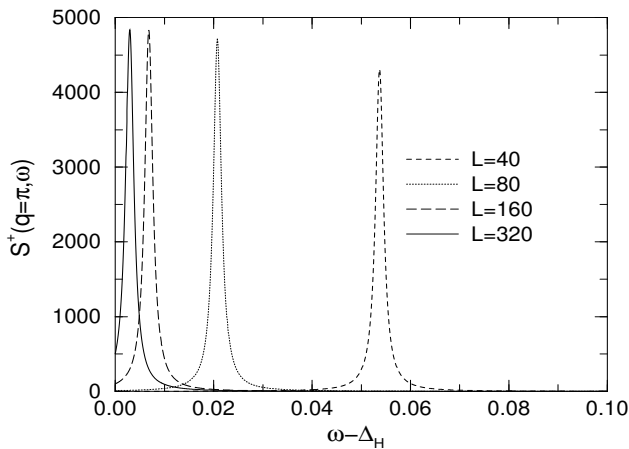


FIG. 5. The single magnon excitation at  $q = \pi$  in spin-1 chains of different length versus the frequency minus the Haldane gap  $\Delta_H$ . Calculations with  $m = 128$  states kept and broadening factor  $\eta = 0.001$

Table II and Fig.6(a) show the weight in the first peak. The weight grows with the system size, but seems to go to  $W_0 = 97.6\% \pm 0.1\%$  instead of 100%. This value is important for estimating how good a single mode approximation for this excitation is.

TABLE II. The weight  $W_0$  of the first peak as a function of the length  $L$  of the spin-1 chain and number  $m$  of states kept.

$L$	$W_0(m = 64)$	$W_0(m = 128)$	$W_0(m = 256)$
40	0.9346	0.9288	0.8415
80	0.9675	0.9617	0.9540
160	0.9753	0.9742	0.9737
320	0.9755	0.9755	0.9756

Table III and Fig. 6(b) show the position of the first peak  $\omega_0$ . We expect this value to converge against the Haldane gap  $\Delta_H = 0.41050(2)$  for big systems. For the  $L = 320$  site chains our result is only 0.7%(128 states) above this value, and Fig. 6(b) indicates that the distance between the Haldane gap and the peak vanishes for big systems.

By determining the frequency at which the first peak is for different wavevectors, we can calculate the single magnon dispersion relation. Figure 7 shows the dispersion relation determined with the Lanczos vector method, as well as quantum Monte Carlo<sup>8</sup> and exact diagonalization<sup>9</sup>. The different sets of data are in good agreement, except for small  $q$ , where the quantum Monte Carlo results are smaller than ours.

In summary, we have shown that the Lanczos vector method works very well for the dynamical spectrum of the antiferromagnetic spin-1 Heisenberg model.

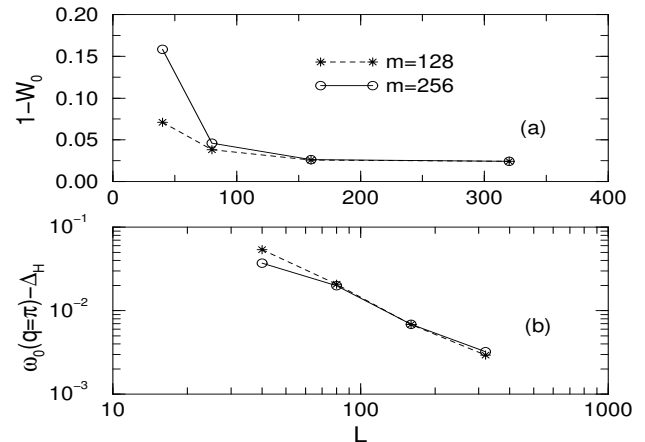


FIG. 6. The upper plot (a) shows the weight of the first peak  $W_0$  versus the system size  $L$ . The lower plot (b) shows the difference of the frequency of first peak  $\omega_0$  and the Haldane gap  $\Delta_H$ . The difference tends to zero as the system size increases.

TABLE III. The position of the first peak  $\omega_0$  as a function of the length  $L$  of the spin-1 chain and number  $m$  of states kept.

$L$	$\omega_0(m = 64)$	$\omega_0(m = 128)$	$\omega_0(m = 256)$
40	0.4657	0.4642	0.4477
80	0.4326	0.4313	0.4304
160	0.4192	0.4173	0.4174
320	0.4159	0.4134	0.4137

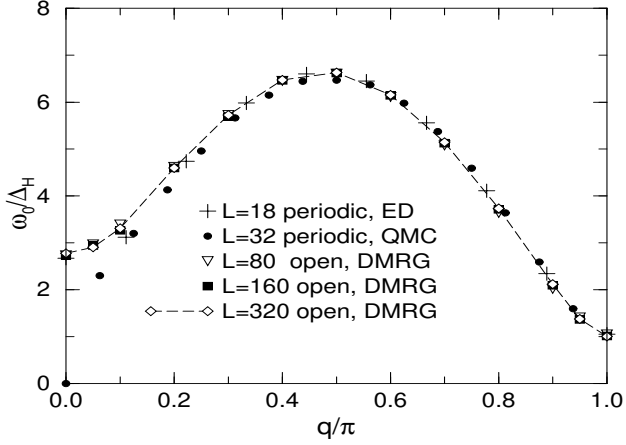


FIG. 7. The single magnon line of the Spin 1 Heisenberg antiferromagnet. DMRG results with  $m = 128$  states per block, and three Lanczos vectors as target states. Quantum Monte Carlo(QMC)<sup>8</sup> and exact diagonalization<sup>9</sup>(ED) data are from the work of Takahashi.

## V. THE SPIN-1/2 HEISENBERG MODEL

As we have already pointed out, the spin-1 chain is a relatively easy case. Since there is an excitation gap and the correlation length is short, the ground state properties can be calculated with high accuracy with a relatively small DMRG basis. Following the example of Hallberg<sup>3</sup>, we now investigate the antiferromagnetic spin-1/2 chain. This is a more difficult case, since it has no excitation gap and a diverging correlation length, requiring a slightly bigger DMRG basis. More importantly, instead of a single peak with most of the weight in it, for  $S^+(\omega, q)$  an excitation band is found. It has a lower boundary<sup>10</sup>

$$\omega_q^l = \frac{\pi}{2} | \sin(q) |, \quad (20)$$

and upper boundary<sup>11</sup>

$$\omega_q^u = \pi | \sin(q/2) |. \quad (21)$$

For this band the following structure was proposed<sup>12</sup>:

$$S^{zz}(q, \omega) = \frac{A}{\sqrt{\omega^2 - \omega_q^l{}^2}} \Theta(\omega - \omega_q^l) \Theta(\omega_q^u - \omega). \quad (22)$$

In a finite chain there can be no continuous energy band. Instead, we expect separate peaks in the same region, and that the number of peaks increases as the system size is increased.

This poses a problem to the Lanczos vector method. Figure 3 shows that the weight of the Lanczos vectors in the spectral weight function decreases only very slowly. This means that a lot of Lanczos vectors are needed to describe the correlation function well. Figure 8 shows

the spectral weight at  $q = \pi$  determined with different numbers of Lanczos vectors. For reference we also show results using the much more accurate correction vector method, discussed in the next section. The spectral weight function strongly depends on the number of Lanczos target states, and even for 16 and 32 Lanczos vector target states there is no sign of convergence. Bigger numbers of target states  $N_L$  would result in very long calculation times, and would also require that we keep substantially more states per block.

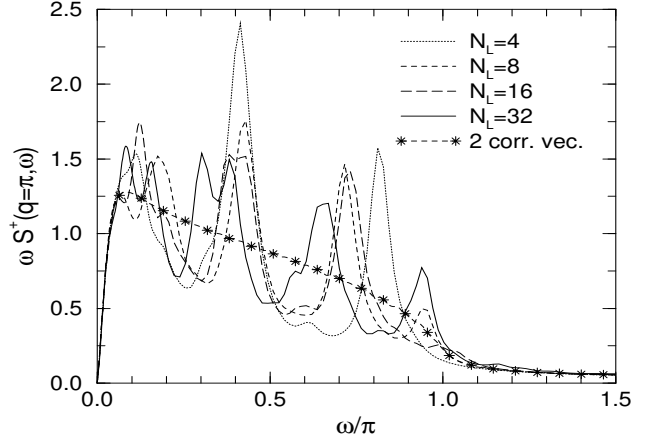


FIG. 8. The spectral weight function at  $q = \pi$  in a 160 site spin-1/2 chain with  $\eta = 0.1$  for calculations with different numbers of Lanczos target state  $N_L$  and with the correction vector method. In all calculations  $m = 256$  states were kept in the DMRG basis. The correction vector method works well, while the Lanczos method is far from convergence.

While the high energy part of the spectral weight function is not accessible with the Lanczos vector method, the position of the first peak is only weakly dependent on the number of Lanczos vector target states  $N_L$ . Table IV shows the position of the first peak  $\omega_0$  in a  $L = 160$  site chain at  $q = \pi$  calculated with  $m = 256$  states kept. The dependence of the position of the first peak on the number of Lanczos vector target states is small. The reason why it is shifted to higher values if more target states are used are the increasing truncation errors arising from targeting more states with fixed  $m = 256$ .

TABLE IV. The position of the first peak  $\omega_0$  depending on the number of Lanczos vector target states  $N_L$  in the spectral weight function of an antiferromagnetic  $L = 160$  site spin-1/2 chain at  $q = \pi$ .  $m = 256$  states were kept in the DMRG basis.

$N_L$	$\omega_0$	$P$
4	0.0269	$9.4 \times 10^{-8}$
8	0.0297	$6.2 \times 10^{-6}$
16	0.0380	$1.5 \times 10^{-4}$
32	0.0644	$6.9 \times 10^{-4}$

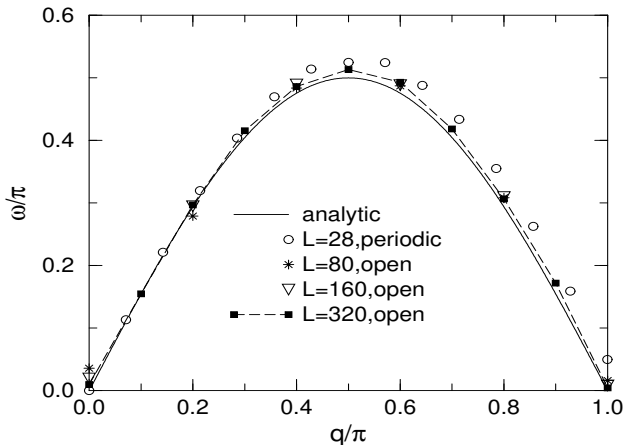


FIG. 9. The lower bound of the excitation band in the Spin 1/2 Heisenberg model. The results for the 28 site periodic system are from Hallberg<sup>3</sup>.

Keeping  $m = 256$  states in the DMRG basis, and targeting four Lanczos vectors, we have determined the lower edge of the energy band for different  $q$ . Figure 9 shows the dispersion relation. For the longer systems it compares increasingly well with the analytic result (Eq. 20).

## VI. CORRECTION VECTORS

In the previous section we found that the Lanczos vector method works very well if only low-energy properties of the dynamical correlation function are of interest, but that it is unable to reproduce higher energy properties like the shape of the excitation band in the spin-1/2 model. Instead of using the Lanczos vector method, the spectrum can be calculated directly for a given  $z = \omega + i\eta$  by using a correction vector. To do this, the following states must be included as target states:

$$\begin{aligned} |0\rangle & \quad \text{the ground state} \\ |A_q\rangle & = A_q |0\rangle \quad \text{the first Lanczos vector} \\ |x(z)\rangle & = \frac{1}{z-H} |A_q\rangle \quad \text{the correction vector} \end{aligned}$$

Since a finite broadening factor  $\eta$  is used, the correction vector becomes complex. To avoid the use of complex numbers, we split the correction vector into real and imaginary part, both used as target states:

$$|x(z)\rangle = |x^r(z)\rangle + i|x^i(z)\rangle. \quad (23)$$

The equation for the correction vector is split into real and imaginary parts  $|x^r(z)\rangle$  and  $|x^i(z)\rangle$ , and the imaginary part is found by solving

$$((H - \omega)^2 + \eta^2) |x^i(z)\rangle = -\eta |A_q\rangle \quad (24)$$

using the conjugate gradient method. Note that this equation system gets more singular as  $\omega$  gets closer to

an eigenenergy of the Hamiltonian, and as the broadening factor  $\eta$  gets smaller. For large  $\eta$  the Hamiltonian is close to a diagonal matrix, and the conjugate gradient method converges much faster than for small  $\eta$ . This means that a large  $\eta$  results in short calculation times, but it also limits the resolution of the spectrum. The convergence is also slowed down because energy gaps in  $H - \omega$  are squared in Eq. (24), and the convergence rate of the conjugate gradient method depends on the gap between the lowest and the next lowest eigenvector.

The real part of the correction vector is calculated directly:

$$|x^r(z)\rangle = \frac{1}{\eta} (\omega - H) |x^i(z)\rangle; \quad (25)$$

Using the correction vector, the Green's function can be calculated directly:

$$G(q, z) = \langle A_q | x(z) \rangle \quad (26)$$

Taking these states ( $|0\rangle, |A_q\rangle$  and  $|x(z)\rangle$ ) as target states and optimizing the DMRG basis to represent them allows for a very precise calculation of the Green's function for a given frequency  $\omega$  and broadening factor  $\eta$ . Unfortunately, the correction vector has to be calculated separately for every  $\omega$ . If the correction vector does not change very rapidly with  $\omega$ , the DMRG basis that is optimized to represent the correction vector at a certain  $\omega$ , should also be able to represent correction vectors for nearby frequencies.

Although the correction vectors are needed as target states to determine the DMRG basis, it is more efficient to use the Lanczos vector method to determine the complete spectra within that basis. Using the correction vector, but no Lanczos vectors except the first one, as a target state, DMRG sweeps are performed until the basis is converged (typically two or three sweeps). The dynamical correlation function is then calculated in the same way as in the Lanczos vector method: when the left and right block have the same size Lanczos vectors are calculated until orthogonality is lost. Since this method is almost exact in the given basis, in principle it should yield the same result as using the correction vector method in the same basis, and it is much faster. Of course, while the spectrum is produced for all  $\omega$ , it is only accurate near the  $\omega$  used to produce the correction vector.

To determine the range of  $\omega$  in which the truncated basis is good enough to calculate the spectral function, we compare calculations with different frequencies for the correction vectors. Figure 10 shows the spectral weight function near the upper edge of the excitation band in the antiferromagnetic spin-1/2 chain. This is an especially difficult region, because there are a lot of peaks at lower energies. We did several calculations with correction vectors for different  $\omega$ , calculating the spectral weight in the region around the targeted frequencies. With  $m = 128$  states kept, the overall shape reproduces the edge of the band accurately. Deviations between the pieces of the

spectrum calculated with different correction vectors can be seen. The small mismatch between the very accurate values calculated directly from the correction vectors, and the corresponding part obtained with the Lanczos vector method are due to numerical errors in the Lanczos procedure. By keeping more states this result can be improved. Figure 11 shows the same part of the spectrum with  $m = 256$  states kept. Now the different parts match very well. Further improvement would be possible by keeping more states or reducing the distance between the frequencies of the correction vectors.

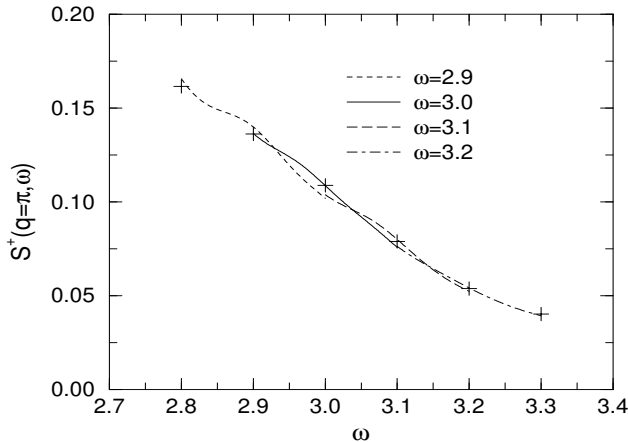


FIG. 10. The spectral weight in a 80 site spin-1/2 chain at  $q = \pi$  with one correction vector as a target state and 128 states in the DMRG basis and  $\eta = 0.1$ . The crosses show the results calculated directly from the correction vectors, the lines show the parts calculated with the Lanczos procedure in the basis optimized for the correction vectors. For example, the dashed line from  $\omega = 2.8$  to  $\omega = 3.0$  is calculated in the basis that is optimized for the correction vector with  $\omega = 2.9$ .

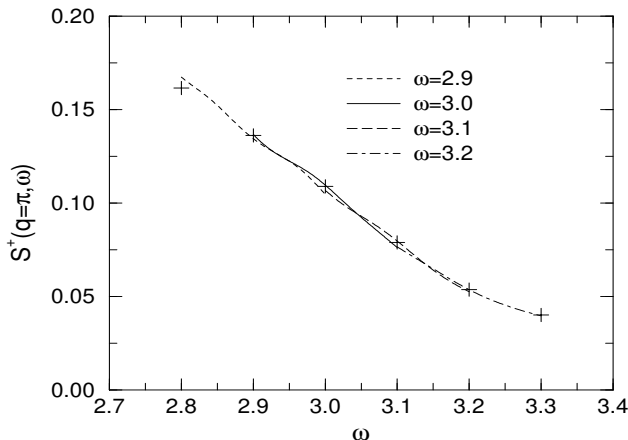


FIG. 11. The spectral weight in a 80 site spin-1/2 chain at  $q = \pi$  with one correction vector as a target state and 256 states in the DMRG basis and  $\eta = 0.1$ .

This result can be improved even further. Instead of using just one correction vector as a target state, we try

using two correction vectors at the same time. The spectral weight can then be interpolated for frequencies between these two correction vectors. With a broadening factor of  $\eta = 0.1$ , a distance of  $\Delta\omega = 0.2$  between the two correction vectors seems appropriate. In Fig. 12 and 13 the results from calculations with different frequencies for the correction vectors are plotted. With  $m = 128$  states the parts for  $3.0 \leq \omega \leq 3.3$  match perfectly, and for  $2.8 \leq \omega \leq 3.0$  they still match better than with only one correction vector as a target state (Fig. 10). With  $m = 256$  states (Fig. 13) all pieces of the spectrum match up almost perfectly. This gives us a consistent method to verify how good our numerical results are, and we find that it is possible to achieve very high accuracy.

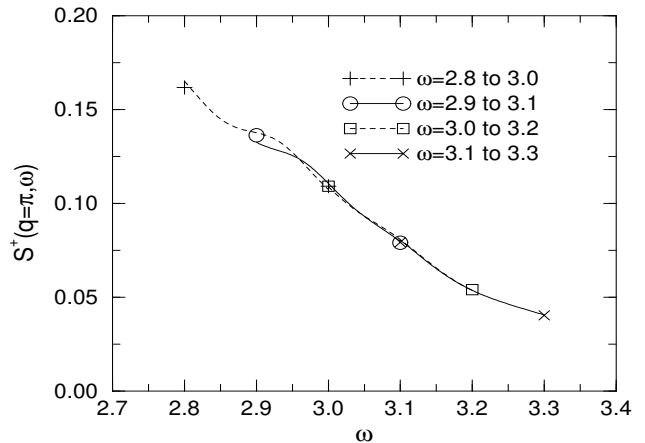


FIG. 12. The spectral weight function in a 80 site spin-1/2 chain at  $q = \pi$ , with 128 states in the DMRG basis and  $\eta = 0.1$ . Two correction vectors are used as target states, and the plot shows the values calculated directly with these correction vectors, and the connecting lines show the interpolated spectral weight calculated with the Lanczos procedure in the basis optimized for the correction vectors.

Now we use this method to obtain the complete spectral weight in a 160 site chain. Keeping  $m = 256$  states and using two correction vectors as target states, we start with correction vectors for  $\omega = 0$  and  $\omega = 0.2$ . After two sweeps through the system the DMRG basis is converged, and the spectral weight function is calculated for  $0 \leq \omega \leq 0.2$  using the Lanczos procedure. Then we target  $\omega = 0.2$  and  $\omega = 0.4$ , perform two sweeps through the system, and calculate the spectral weight for  $0.2 \leq \omega \leq 0.4$ . Continuing this procedure, we obtain the function shown in Fig. 8. In contrast to the results from the Lanczos vector method, the spectral weight function calculated using two correction vectors shows no finite-size peaks and reflects the shape expected in the infinite system. Eq. (22) predicts  $1/\omega$  decay from  $\omega = 0$  to  $\omega = \pi$ , where the spectral weight drops to zero. The band presented in Fig. 8 shows the correct upper and lower bound, but the spectral weight in the band decays faster than  $1/\omega$ . To verify if this is a finite-size effect,



we look at chains with different lengths. Figure 14 shows that the spectral weight decays faster than  $1/\omega$  in all system, and the decays do not become slower for longer chains. The only hint at finite-size effects is the different size of the spectral weight for different system sizes.

The small oscillations in the 40 site chain are due to the limited number of peaks in the relatively small system, those in the 160 site chain are due to the large distance of  $\Delta\omega = 0.4$  between the correction vectors. They do not affect our result, and could be removed by using pairs of correction vectors with closer frequencies or by increasing the size of the DMRG basis.

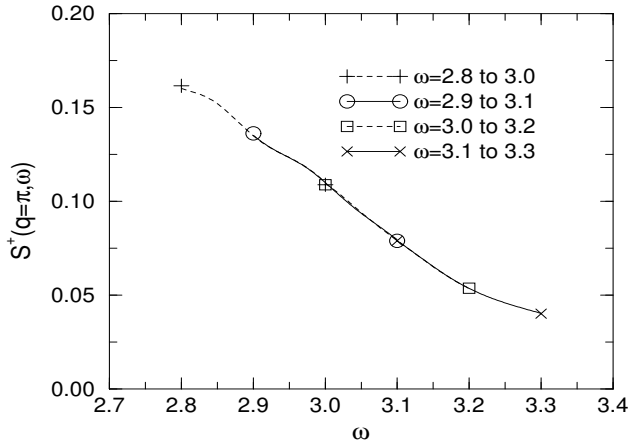


FIG. 13. The spectral weight function in a 80 site spin-1/2 chain at  $q = \pi$ , with 256 states in the DMRG basis and  $\eta = 0.1$ . Two correction vectors are used as target states, and the plot shows the values calculated directly with these correction vectors, and the connecting lines show the interpolated spectral weight calculated with the Lanczos procedure in the basis optimized for the correction vectors.

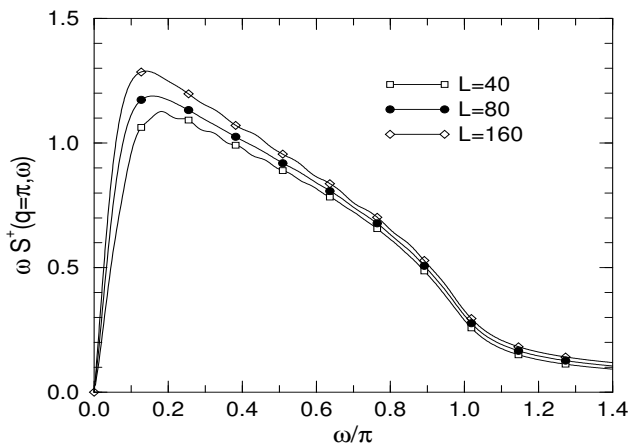


FIG. 14. The spectral weight function at  $q = \pi$ , with different system sizes. The spectra were calculated with two correction vector target states with distances of  $\Delta\omega = 0.4$ , a broadening factor  $\eta = 0.2$  and  $m = 256$  states.

In Fig. 13 the upper edge of the excitation band can be seen, but due to the broadening factor  $\eta = 0.1$  it is difficult to determine the position of the edge. Since the spectral weight function is plotted by taking the peaks found in the Lanczos procedure and plotting them with the given  $\eta$ , they can as well be plotted with smaller broadening factors. Figure 15 shows plots with  $\eta = 0.1$ , for which the DMRG basis was optimized, and  $\eta = 0.05$  and  $\eta = 0.01$ . For the smaller  $\eta$  the different parts of the spectral weight function no longer match, but now the poles are easily identifiable. The position of the peaks can also be determined by directly taking the position of the peaks from the Lanczos procedure. Doing this, the last peak in the band is found at  $\omega = 3.128$ , compared to  $\omega = \pi$  given in (Eq. 21). To verify if the small difference is a finite-size effect or a numerical error, longer chains can be studied, or correction vectors closer to the desired region could be used. Using smaller  $\eta$  and reducing the distance between the correction vectors also gives higher resolution.

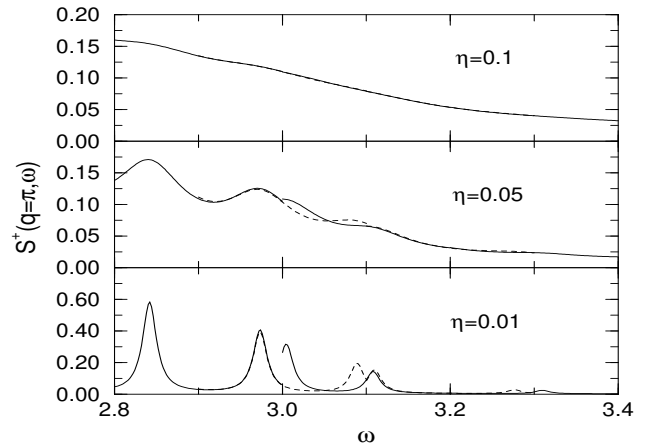


FIG. 15. The spectral weight function in a 80 site chain at  $q = \pi$ . This is the same data as in figure 13, with two correction vectors with a distance of  $\Delta\omega = 0.2$  between them, and  $\eta = 0.1$ . If the spectral weight function is plotted with a smaller  $\eta$ , the parts calculated with different frequencies for the correction vectors no longer match perfectly, but the peaks become easily distinguishable.

## VII. CONCLUSIONS

In conclusion, we have presented and tested two methods to calculate dynamical correlation functions using DMRG. We have shown that the Lanczos vector method works very well if only the low-energy part of the correlation function is of interest, or if the bulk of the weight is in one single peak. We demonstrated this for the case of the antiferromagnetic spin-1 and spin-1/2 chains, where we could reproduce the dispersion relation of the lower edge of the spectral weight functions correctly.

If there is an excitation band, the Lanczos vector method is unable to describe the higher energy part of the correlation functions. These parts can be determined using the correction vector method. This method gives very precise results for frequencies at which the correction vectors are used as target states. The Lanczos procedure can be used in the basis optimized for the correction vectors to determine the spectrum fast and efficiently not only at the frequency of the correction vector, but also in the region around that. By comparing the plots from calculations with different frequencies for the correction vectors it is possible to estimate the range over which the spectral function is determined correctly. We find that remarkably good spectra can be determined if two correction vectors are used as target states, and the spectral function is calculated for the frequencies between them. In the case of the excitation band in the spectral weight function of the antiferromagnetic spin-1/2 chain, we used this method and were able to study a system long enough and with sufficient accuracy that no finite-size peaks were visible and excellent agreement with theoretical expectations was obtained.

Our results show that using these techniques, obtaining accurate dynamical spectral functions from DMRG is feasible and can be considered a standard DMRG technique. The calculation time is longer than for ground state properties, but still manageable for single chain systems and probably for ladders with a few chains.

## VIII. ACKNOWLEDGMENTS

The authors would like to thank H. Monien, E. Jeckelmann and S. K. Pati for profitable discussions. We are especially grateful to M. S. L. du Croo de Jongh for discussions and program design and development. This work was supported by the National Science Foundation under grant DMR98-70930 and the DAAD “Doktorandenstipendium im Rahmen des gemeinsamen Hochschulsonderprogramms III von Bund und Ländern”.

- <sup>9</sup> Minoru Takahashi, Phys. Rev. B **48**, 311 (1993).  
<sup>10</sup> J. des Cloiseaux and J. J. Pearson, Phys. Rev. **128**, 2131 (1962).  
<sup>11</sup> T. Yamada, Prog. Theor. Phys. Jpn. **41**, 880 (1969); L. D. Eaddeev and L. A. Takhtajan, Phys. Lett. A **85 A**, 375 (1981).  
<sup>12</sup> Gerhard Müller, Harry Thomas, Hans Beck and Jill C. Bonner, Phys. Rev. B **24**, 1429 (1981).

---

<sup>1</sup> Steven R. White, Phys. Rev. Lett. **69**, 2863 (1992).

<sup>2</sup> Steven R. White, Phys. Rev. B **48**, 10345 (1993).

<sup>3</sup> Karen A. Hallberg, Phys. Rev. B **52**, 9827 (1995).

<sup>4</sup> Z. G. Soos and S. Ramasesha, J. Chem. Phys. **90**, 1067 (1989).

<sup>5</sup> S. Ramasesha, S. K. Pati, H. R. Krishnamurthy, Z. Shuai, J. L. Bredas, Synth. Metals **85**, 1019 (1997).

<sup>6</sup> Ian Affleck, Tom Kennedy, Elliot H. Lieb and Hal Tasaki, Phys. Rev. Lett **59**, 799 (1987).

<sup>7</sup> Steven R. White and David A. Huse, Phys. Rev. B **48**, 3844 (1993).

<sup>8</sup> Minoru Takahashi, Phys. Rev. Lett. **62**, 2313 (1989).